Pol. J. Environ. Stud. Vol. XX, No. X (XXXX), 1-12
DOI: *10.15244/pjoes/190660* ONLINE PUBLICATION DATE:

Original Research

Removal of Heavy Metals from Wastewater By The Membrane-Adsorbent System With Different Running Methods

Yuxin Qu[1], Xiankun Tang[1], Hongzheng Ren[1], Xiaoya Sun[2], Danni Liu[2], Xiao Wu[3], Liang Xu[1]*

[1]School of Resources and Environment, Qingdao Agricultural University, Qingdao, 266109, China
[2]Advanced Agricultural Technology Institute, Qingdao Agricultural University, Qingdao, 266109, China
[3]International Office of Cooperation & Exchange, Qingdao Agricultural University, Qingdao 266109, China

Received: 20 May 2024
Accepted: 30 June 2024

Abstract

Waste shells can be used to treat wastewater, e.g., livestock and poultry wastewater, containing heavy metals. Shells can be crosslinked with organic compounds to synthesize hydrates with improved adsorption efficiency, which is difficult to separate from wastewater. Percolation membrane and composite adsorbent were prepared using PVA and oyster shell as the main materials to construct a membrane-adsorbent coupled system for the treatment of wastewater with heavy metals. During the treatment process with the coupled system, the adsorbent was not in direct contact with wastewater and could be easily separated. Shell-based adsorbents were less prone to clumping and loss with fluent. The removal of heavy metal ions by modified adsorbent material in the dynamic running method was more than 20 times higher than that of unmodified shell material in the static method. This may be attributed to the surface modification, which improved the surface lubricity of the adsorbent material, coupled with the dynamic adsorption method, which avoided the occurrence of agglomeration of the adsorbent material and enhanced the external mass transfer process of heavy metals to modified adsorbents. The coupled system and dynamic running method have potential applications in treating heavy metal contamination in fecal wastewater in remote rural areas.

Keywords: poly (vinyl alcohol), oyster shell powder, heavy metals, dynamic and static adsorption, modification

Introduction

As a large livestock and poultry breeding country, China's livestock breeding has gradually developed and expanded based on decentralized breeding by small-scale households. In 2020, the scale rate of livestock and poultry breeding in China has already reached 67.5%. Pig breeding is an important part of China's livestock and poultry breeding [1]. In recent years, pig breeding has been further scaled up and industrialized [1, 2], but the proportion of large-scale breeding of 10,000

*e-mail address: xuliang@qau.edu.cn

or more pigs per year is only approximately 18%, and retail breeding still occupies an important proportion of China's pig breeding industry [2].

Heavy metals and antibiotics are widely added to feedstuffs to promote the growth of pigs and prevent diseases. The absorption rate of heavy metals and antibiotics by livestock is low. Hogs can only absorb 10%-20% of Cu and Zn in feed, and 30%-90% of antibiotics cannot be absorbed and metabolized by animals [3, 4]. As a matter of course, a large number of additives are excreted in feces and urine. In particular, certain farmers running small- or medium-scale farms with poor farming techniques and skills may actively overuse heavy metals and antibiotics in the farming process, resulting in high levels of pollutants in the discharged manure and increasingly severe pollution [5]. As heavy metals have the characteristics of low migration, difficult degradation, easy enrichment, and great harm, they may have adverse effects on the ecological environment, the safety of livestock and poultry products, human health, and other aspects [6]. Therefore, it is of great significance to actively prevent and control heavy metal pollution in pig production.

Large-scale hog farms can control the amount of feces production and pollutant concentration through advanced breeding techniques, management models, and supporting waste treatment facilities and equipment [5]. This can, to a certain extent, solve the problems of feces treatment and resource utilization. However, in China's vast rural areas, there are still many pig farmers with small farm sizes ranging from a few dozen to more than a few hundred heads [2]. The distribution of farms in rural areas is relatively decentralized, and it is difficult to connect the feces waste discharged to a unified wastewater and waste treatment system for centralized treatment. In some areas, farmers, either on their initiative or at the request of the management, have constructed a multi-stage sedimentation tank outside the piggery, where solid-liquid separation is performed after feces discharge. The sludge at the bottom of the sedimentation tank is cleaned out and stockpiled in the field or discharged as organic fertilizer into farmland and surrounding waters, becoming one of the sources of agricultural surface pollution.

Adsorption is one of the commonly used techniques in the field of wastewater treatment, with the advantages of simple operation, multiple sources of materials, wide range of concentration applicability, and good effect [6-9]. As known, activated carbon is widely used in a variety of wastewater treatments [10], nano-silica adsorbents can be used for pharmaceutical and dyeing wastewater [11, 12], and modified shells can be used to treat heavy metal pollutants [6, 13-15]. There are some practical problems in the removal of heavy metals with shell-based adsorbents from feces wastewater, especially from small-scale retail breeding. For example, to improve the treatment effect of the adsorbent on heavy metals, the adsorbent is usually put into the wastewater or fermented marsh liquid directly in the form of powder or mixed with excrement. It is difficult to recover the powder adsorbent from the fecal mixture after treatment [6, 13, 14]. As a result, the adsorbent enters the soil and water with feces, and there is a risk that the adsorbed heavy metal pollutants will re-enter the environment.

Shellfish aquaculture is also well-developed in China and generates a huge amount of waste shells every year [16, 17]. The main component of shells is calcium carbonate. Shell powder is a common natural adsorbent material with a large specific surface area, high porosity, low cost, and good treatment effect on heavy metals [7]. Shell powder after acid treatment, heat treatment, or grinding treatment, partially changes the composition of the shell, or shell structure, or makes the porosity-specific surface area increase, improving the adsorption capacity of shell powder on heavy metals [7, 14, 15, 18]. To maximize the adsorption effect of shell powder, the adsorbent is usually used in the form of powder to obtain a large surface area and surface energy, but shell powder is easily lost with water flow and difficult to recycle and reuse [6, 14]. In addition, shell powder tends to clump in water, which reduces the adsorption effect. Modification of shell powder to integrate shell powder into polymeric materials, such as polyvinyl alcohol, and polyethylenimine, as fillers is a viable solution to these problems [6, 9, 19]. Therefore, waste shells can be modified and prepared into organic-inorganic composite adsorbents for the adsorption treatment of heavy metals or dye-polluted wastewater.

In some coastal rural areas, there are large quantities of discarded shells, even forming serious solid waste pollution. These shells and the modified products can be used as potential adsorption materials for farming wastewater. However, if only adsorbents and conventional adsorption methods are used to treat wastewater generated by small-scale retail farming, heavy metals in feces, as well as in digested wastewater and sludge formed by feces fermentation, may re-enter the surrounding water and soil environment. Therefore, it is necessary to develop a new adsorption method to solve the problem of heavy metal pollution in farm wastewater from rural non-centralized discharges. Using the new way, is it possible to remove heavy metal pollutants from feces without directly adding the prepared adsorbent to the feces? This would create good conditions for the subsequent resource utilization of the manure. In addition, the waste shells can also be resourcefully utilized to a certain extent.

Material and Methods

Material

Copper chloride (purity: 99%), zinc sulfate (purity: 99.5%), chromium chloride (purity: 99%), and sodium silicate (purity measured as Na_2O, w%: 19.3-22.8%), PVA (hydrolysis degree: 88%; purity: 99%; molecular weight: 140000 g mol^{-1}), were purchased

from Sinopharm Chemical Reagent Co., Ltd., Shanghai, China. Oyster shells were obtained from the seafood market in Qingdao, Shandong Province, China.

Preparation of the Adsorbent and the Percolation Membrane

Oyster shells were first crushed with a hammer and then washed. The washed crushed oyster shells are put into the ball mill tank and processed for 6 hours. The oyster shell powders (OSP hereafter) were then oven-dried at 70°C to constant weight and stored at room temperature for further use.

A certain amount of PVA was soaked in deionized water for 24 hours, then stirred and heated at 90°C for dissolution. After the dissolving of PVA and naturally cooling, deionized water was added to make a 5 wt% PVA solution. Quantified OSP and sodium silicate were added into the PVA solution, which was then vigorously stirred at 90°C for 2 hours. After that, the mixtures were continuously stirred at room temperature for two hours and cooled. The mixture was left to stand, and solid-liquid separation occurred. The lower solid layer was modified shell powder (MOSP hereafter). The supernatant was poured into Teflon Petri dishes and dried at 40ºC for 24 hours to obtain the percolation membrane (PM hereafter).

Static and Dynamic Adsorption Experiments with Membrane-Adsorbent System

A certain amount of OSP and MOSP were sealed separately in PM to form an 'outer PM bag-inner adsorbent' structure for following static adsorption experiments. In addition to the PM bag, the PM obtained from the supernatant was also made into fine tubes for dynamic adsorption experiments. Pollution solutions, which were used to simulate wastewater contaminated with heavy metals (e.g. fecal effluent from livestock farming), were prepared with $CuCl_2$ and $ZnSO_4$. The OSP, the MOSP, and the outer PM (including bags and tubes) were collected separately at 7 different time points over 12 hours. The collected materials were soaked with hydrochloric acid to extract the heavy metal pollutants, which were used to analyze heavy metal concentrations and adsorption effects, and the associated changes in adsorption data were fitted to different kinetic models. The ion concentrations were measured by ICP-OES (OPTMA8000DV, PerkinElmer, Inc. USA). The water absorption rate (W) of the PM was also measured, as PM has a good water absorption capacity that may affect the adsorption process. A certain mass of dried PM sample (mass was recorded as m_0) was plunged into deionized water, removed from water at certain intervals, the surface water was dried, and the sample mass (m_t) was measured. The Equation for calculating the water absorption rate is shown below:

$$W = \frac{(m_t - m_0)}{m_0} \times 100\% \quad (1)$$

Characterization of Adsorbents

The crystal structures data of the PM, the OSP, and the MOSP were collected by an X-ray diffractometer (TD-3700, Dandong Tongda Science & Technology Co., Ltd., China) with the scanning range 2θ = 10-80° and the scanning increment of 0.02°. The chemical structures of the samples were scanned by an FT-IR spectrometer (Nicolet isl0, Thermo, the USA), with frequencies ranging from 400 cm^{-1} to 4000 cm^{-1}. The surface morphologies of the adsorption materials and membranes were determined using a Field Emission Scanning Electron Microscope (Gemini 500, Carl Zeiss Microscopy Deutschland GmbH, Germany).

Results and Discussion

XRD Analysis

The diffraction pattern of the pure PVA (Fig. 1(a)) indicates diffraction bands around 2θ = 19.6° and 40.7°, representing reflections from (101) and (111) [20]. It is obvious from the XRD figures of PM (Fig. 1(b)) that the relative intensities and areas of two characteristic peaks of the PVA decreased after the embedding of the OSP particles in the PVA matrix. The features clarify a decrease in the crystalline phase of the PVA matrix, implying that the reaction was likely to occur in the hydroxyl groups of PVA. The XRD spectra of the OSP (Fig. 1(c)) clearly show that these samples were mainly composed of calcite, reflected by the diffraction peaks assigned to the (012), (104), (110), (113), (202), (018), and (116) crystallographic planes of calcite, respectively [15]. The XRD pattern for the MOSP (Fig. 1(d)) is similar to that of the OSP, but there are some differences in diffraction intensities and positions of the characteristic peaks. Compared to the OSP, a new small peak appeared in the MOSP around 2θ=19.9°, corresponding to reflections from (101), which might be related to the incorporation of the hydroxyl group. Main peaks assigned to calcium silicate hydrate were observed around 2θ = 29.9° (110), 32.0° (200), and 49.0° (020), respectively [19].

FT-IR Analysis

Changes in the chemical interaction between the components of the modified materials can be initially investigated by FT-IR spectrometer. For the pure PVA (Fig. 2(a)), the wide and intense band between 3000 to 3600 cm^{-1} was observed, which corresponded to the existence of a hydroxyl group with intra- and inter-molecular hydrogen bonding in the PVA chain [21, 22]. The OSP is mainly composed of calcium carbonate

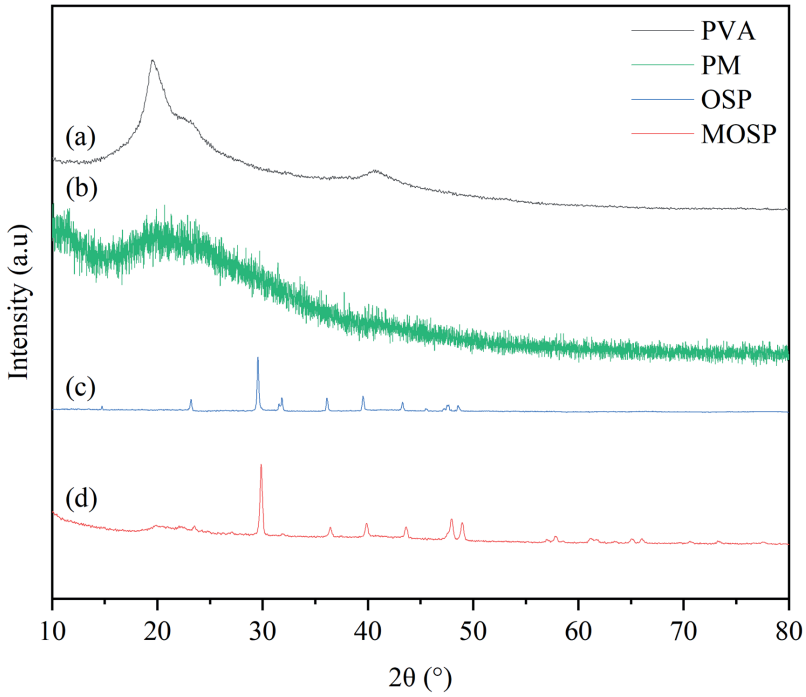

Fig. 1. XRD patterns of (a) the pure PVA, (b) the PM, (c) the OSP, and (d) the MOSP.

in the form of calcite with observed characteristic peaks in Fig. 2(c) centering at 712 (in-plane bending), 873 (out-of-plane bending), and 1405 cm^{-1} (asymmetric stretching), corresponding different stretching vibration peaks of O–C–O, respectively [23, 24]. From the spectra of the PM, new peaks appeared around 2517 (hydrogen-bonded O-H stretch), 2159 (C≡C stretch), and 1560 (-COO^- stretch) cm^{-1} in the PM (Fig. 2(a) and 2(b)). Moreover, the new peaks around 1977 and 2031 cm^{-1} were a quartz matrix signature, indicating the SiO_2 combination band [25-27]. The slightly broader and more intense peak at 1405 cm^{-1}, referring to the vibration modes of CO_3^{2-}, was detected, which was likely to be related to the attendance of the OSP particles coated on the surface of the PVA (Figs. 2(b)). Compared to the OSP, the three characteristic peaks of the calcite in the MOSP shrank significantly (Figs. 2(c) and 2(d)). After modification treatment, some new strong peaks appeared in the MOSP, as illustrated in Fig. 2(d). The MOSP displays new adsorption bands at 1000-1156 cm^{-1} (silicate Si-O stretching), which may be related to the formation of new functional -Si-O-Ca- group [27]. The formation of a hydrated calcium silicate structure has excellent cation exchange capacity, which is conducive to the removal of heavy metal ions. The absorption peaks from 2984 to 3680 cm^{-1} represent the hydroxyl group (O-H, stretching vibration) and silanol groups (Si-OH) mostly located at the surface of the OSP particles, suggesting the combination of the hydroxyl group with the OSP [28]. The new peak at 2917 cm^{-1}, assigned to the C-H stretching vibration, the new peak at 1648 cm^{-1}, attributed to the C-C group based on intra- and inter-molecular hydrogen bonding with the adjacent O-H group, and the new peak at 1556 cm^{-1} [25], associated with the stretching vibrations of -COO^- [27], were observed clearly. Those changes indicate that the OSP and the PVA were successfully crosslinked.

SEM Analysis

The microstructures of the OSP and the modified MOSP are significantly different in shape and size of the observed parts (Fig. 3(a) and 3(b)). The natural oyster shells are mainly composed of a large number of prismatic layers (Fig. 3(a)). The OSP used in the experiments was obtained by ball mill pulverization, and thus both distinct rhombic and rounded portions were present, forming an uneven composite surface structure (Fig. 3(a)). After surface modification to obtain the MOSP, the outer layer presents a reduced overall particle size and some pores could be observed (Fig. 3(b)). The adsorption capacity of heavy metal ions is relatively low due to the fact that OSP tends to accumulate together, thus preventing the full exchange of heavy metal ions and Ca^{2+}. The stacking of flexible organic components on the OSP surface by cross-linking indicates that the OSP material was well modified and might change the characteristics of the OSP, such as water absorption, wettability, and aggregation. Heavy metal ions could pass through the pores on the surface of the organic components, which greatly increases the contact opportunities with Ca^{2+} and ultimately improves the adsorption capacity of the composites for heavy metal ions [14]. On the PM surface, some prismatic OSP particles were deposited (Fig. 3(c)), which might cover some small voids [19]. Due to the

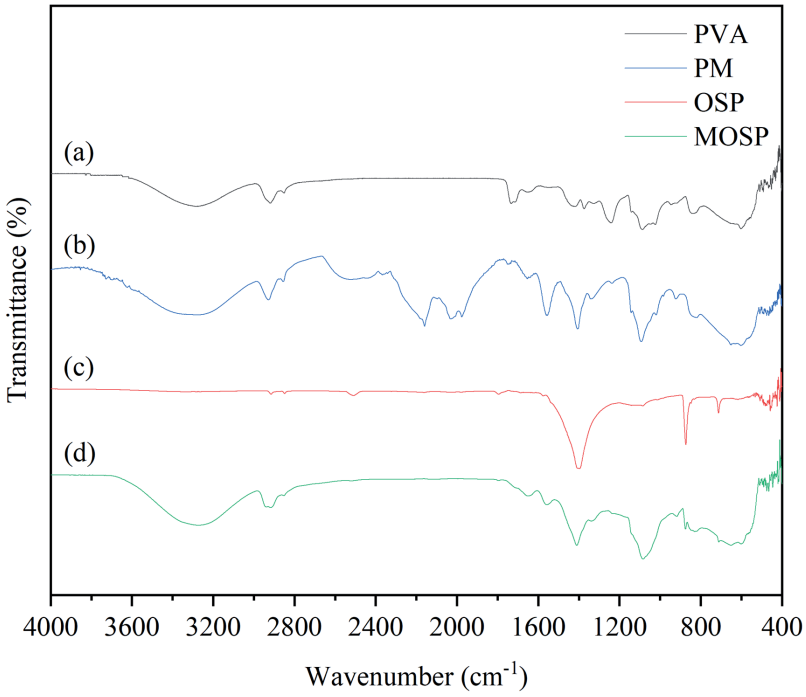

Fig. 2. FT-IR spectra of (a) the pure PVA, (b) the PM, (c) the OSP, and (d) the MOSP.

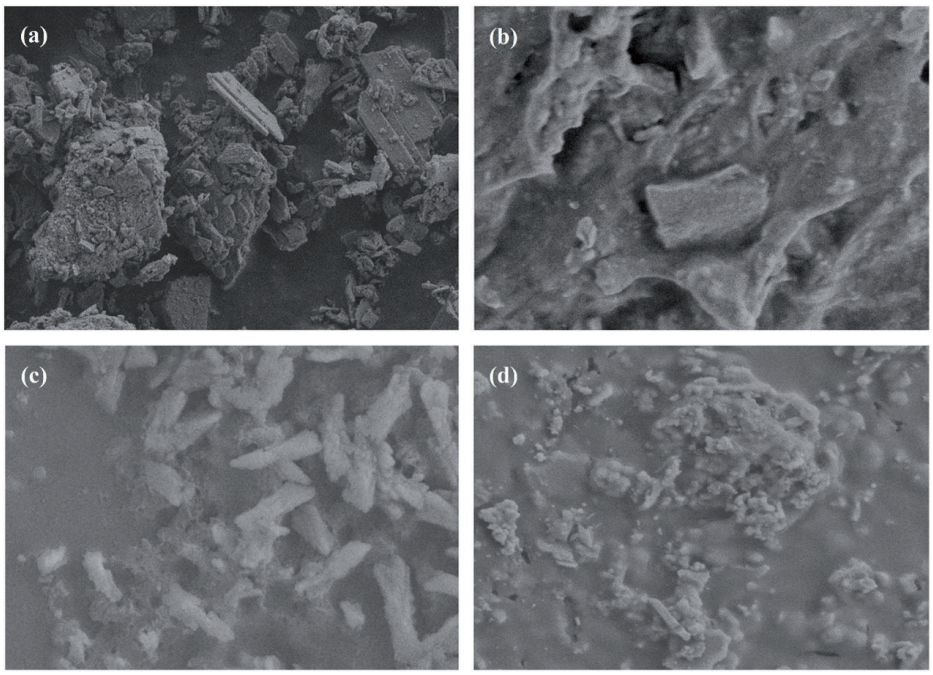

Fig. 3. The SEM micrographs of (a) the OSP, (b) the MOSP, (c) the PM before adsorption, and (d) the PM after adsorption.

aggregation of particles, some larger pores were created [19]. After adsorption occurred, some heavy metal ions were deposited on the OSP particles on the membrane surface, which changed the appearance and shape of the particles (Fig. 3(d)). In addition, the membrane deformed after absorbing water, and the channel pores on the membrane surface deformed as well (Fig. 3(d)).

Adsorption Kinetics and Mechanism

Adsorption is one of the most important methods for eliminating heavy metals from water/wastewater [7, 29]. The adsorption kinetic can provide a theoretical basis for adsorption reaction pathways to help understand the relevant adsorption mechanisms [30, 31]. The equilibrium adsorption processes are described by the pseudo-first-order (Equation 2), pseudo-second-order

kinetics (Equation 3), Elovich (Equation 4), and intraparticle diffusion models (Equation 5) as follows:

$$q_t = q_e(1-e^{-k_1 t}) \quad (2)$$

$$q_t = \frac{k_2 t q_e^2}{1+k_2 t q_e} \quad (3)$$

$$q_t = \frac{1}{b}\ln(1+abt) \quad (4)$$

$$q_t = k_i t^{\frac{1}{2}} + c \quad (5)$$

where q_e and q_t refer to the amount of heavy metal ions adsorbed (mg g^{-1}) at equilibrium and time t (min), respectively; k_1 (min^{-1}), k_2 (g mg^{-1} min^{-1}) and k_i (g mg^{-1} $min^{\frac{1}{2}}$) represent the pseudo-first-order, pseudo-second-order, and intraparticle diffusion rate constants, respectively; a is the initial adsorption rate constant of the Elovich model (mg g^{-1} h^{-1}); b is the Elovich constant (g mg^{-1}); and c is the intercept [9, 30, 31]. Software Origin (Originlab Corporation, Massachusetts, the USA) was used for figure plotting and curve fitting to get each parameter value.

If powdered adsorbents with a large specific surface area, such as shell powder, are added directly to the wastewater treatment system, it can easily lead to the loss of the adsorption materials [6, 14]. There are many ways to solve the problem of adsorbent loss, such as preparing the adsorbent material as nanofiber material or filling the adsorbent material to make a nanocomposite membrane [20, 32, 33]. The solution proposed in this study is to use the PM with good water absorption properties to encapsulate different adsorbents, and to conduct the adsorption process in different ways. The pollutants should first pass through the percolation membrane before coming into contact with the adsorbents for an adsorption reaction. It could be deduced that 1) the outer membrane PM could interact with heavy metal ions in the aquatic environment, 2) the physicochemical properties of the OSP and the MOSP (e.g. specific surface area, surface chemical composition, surface morphology, etc.) may influence the adsorption process, and 3) the between/external/internal mass transfer process involving both the PM and adsorption materials could affect the adsorption rate of heavy metal ions onto the adsorbents.

Before the heavy metal ions came into contact with the mobile adsorption materials inside the membranes, i.e. the OSP and the MOSP, they first passed through the membrane PM. It should be noted that some of the cationic ions would be trapped before passing through the PM due to the deposition and/or cross-linking of the OSP particles on the surface of the PM (Fig. 3(c) and 3(d)). As shown in Fig. 4, the PM had a high water absorption capacity. Water absorption increased rapidly during about the first 100 minutes and then gradually reached saturation (Fig. 4). The adsorption of Cu^{2+} and Zn^{2+} in the PM increased in the pre-adsorption period, then gradually decreased, and finally reached a certain equilibrium (Fig. 4). In the dynamic adsorption process, the accumulation rate of heavy metal ions in the PM was higher than that in the static adsorption process (Fig. 4). The increase in the concentration of heavy metal ions in the PM within a certain time range was likely to be related to the water absorption and adsorption running method of the PM.

The parameters of kinetic models as well as the correlation coefficients (R^2) values of the OSP and the MOSP are presented in Table 1. Overall, the adsorption capacity of the adsorbent materials (the OSP and the MOSP) as well as the PM for copper were all slightly stronger than that for zinc (Table 1; Fig. 4, 5, and 6). In addition, the MOSP showed a stronger adsorption capacity for heavy metals than the OSP (Table 1; Fig. 4, 5, and 6). In the pseudo-first-order model, the pseudo-second-order model, and the intraparticle diffusion model, the higher the rate constant k, the faster the adsorption rate of heavy metal ions. The R^2 values of the MOSP of the pseudo-second-order model are higher than those of the pseudo-first-order model (Table 1), suggesting the fact that the pseudo-second-order model could predict the adsorption behaviors better throughout the whole process with those adsorbents. As the common empirical models, the pseudo-first-order and pseudo-second-order kinetic models can often be used to model the entire system and assume a constant concentration of adsorbate in solution in a heterogeneous system [30, 31]. The constant concentration is of course only an approximation since the concentration of adsorbate in solution decreases as the amount adsorbed decreases. The pseudo-first-order kinetic model is related to the adsorption process being only dependent on the adsorbate concentration-diffusion-controlled process [34]. The pseudo-second-order kinetic model can fit a large amount of kinetic data from different systems, and the model is independent of the specific adsorption mechanism [31].

Comparing the pseudo-first-order model as well as the pseudo-second-order model with the Elovich model, it is found that the R^2 values of the Elovich model were greater than those of the kinetic models in the dynamic adsorption process (Table 1). The Elovich model, commonly used to describe the surface chemisorption process of inhomogeneous adsorbents [30, 31], fits the dynamic adsorption data better than the pseudo model. The model assumes that the adsorption rate decreases over time due to increasing surface coverage and is applicable far from equilibrium [10].

By combining the continuous or segmented fitting curves of the above four kinetic models as well as relevant parameters, it is obtained that the adsorption of both Cu^{2+} and Zn^{2+} by the OSP and the MOSP through static and dynamic adsorption seemed to involve

Table 1. Kinetic parameters of the pseudo-first-order, pseudo-second-order kinetic, Elovich, and intraparticle diffusion models for the adsorption of Cu^{2+} and Zn^{2+} by the OSP and the MOSP.

Material	Adsorbate	Method of adsorption	Pseudo-first-order model			Pseudo-second-order model			Elovich model		
			q_e mg g^{-1}	k_1 min^{-1}	R^2	q_e mg g^{-1}	k_1 g mg^{-1} min^{-1}	R^2	a mg g^{-1} min^{-1}	b g mg^{-1}	R^2
OSP	Cu^{2+}	Static	0.0484	0.0091	0.9565	0.0586	0.1640	0.9748	0.0008	68.5550	0.9610
		Dynamic	1.1621	0.0532	0.6977	1.2395	0.0687	0.9270	2.7040	7.3135	0.9657
	Zn^{2+}	Static	0.0376	0.0106	0.9509	0.0450	0.2507	0.9699	0.0008	92.5266	0.9508
		Dynamic	1.0344	0.0478	0.7054	1.1092	0.0664	0.9284	1.3004	7.5748	0.9687
MOSP	Cu^{2+}	Static	0.0509	0.0135	0.9035	0.0586	0.2789	0.9717	0.0019	82.7914	0.9960
		Dynamic	1.3052	0.0854	0.5817	1.3664	0.1193	0.9030	191.5718	9.8841	0.9553
	Zn^{2+}	Static	0.0443	0.0138	0.9368	0.0510	0.3260	0.9796	0.0017	95.4284	0.9786
		Dynamic	1.1404	0.0772	0.6718	1.1979	0.1179	0.9399	55.2951	10.2955	0.9559

Material	Adsorbate	Method of adsorption	Intraparticle diffusion model					
			$k_{i,1}$ (mg g^{-1} min$^{1/2}$)	c (mg g^{-1})	R^2	$k_{i,2}$ (mg g^{-1} min$^{1/2}$)	c (mg g^{-1})	R^2
OSP	Cu^{2+}	Static	0.0056	-0.0185	0.9763	0.0013	0.0191	0.9657
		Dynamic	0.0501	0.5760	0.9641	0.0088	1.0380	0.9584
	Zn^{2+}	Static	0.0046	-0.0145	0.9431	0.0009	0.0173	0.9775
		Dynamic	0.0476	0.4680	0.9970	0.0075	0.9326	0.9460
MOSP	Cu^{2+}	Static	0.0031	0.0036	0.9992	0.0010	0.0296	0.9997
		Dynamic	0.0392	0.8749	0.9284	0.0067	1.2230	0.9972
	Zn^{2+}	Static	0.0030	0.0009	0.9860	0.0007	0.0293	0.9976
		Dynamic	0.0374	0.7248	0.9326	0.0065	1.0543	0.9286

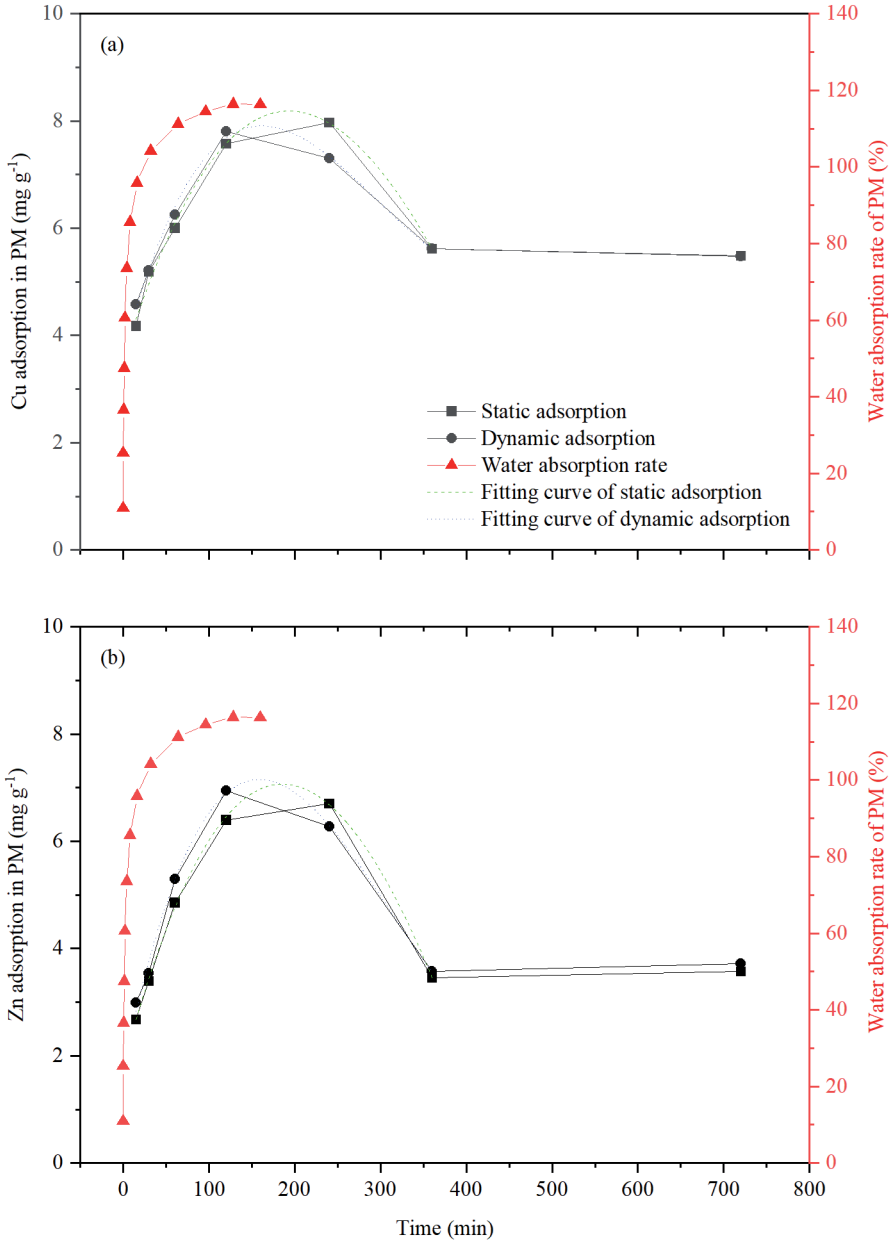

Fig. 4. Shown in the left Y-axis, the adsorption kinetics of Cu^{2+} (a) and Zn^{2+} (b) by the PM with the OSP (black square) and the MOSP (black dot), respectively, as well as the fitting curves of static adsorption (green dashed line) and dynamic adsorption (blue dotted line). Shown in the right Y-axis is water absorption of the PM (red triangle).

different steps. In the static adsorption processes, the q_e of the OSP increased rapidly in the first 60 minutes, while the MOSP increased faster in the first 120 minutes (Table 1; Fig. 6). For dynamic adsorption, on the other hand, the adsorption rates of heavy metal ions by the adsorbent materials were faster in the first 120 minutes (Table 1; Fig. 6). Furthermore, the *a* values of the MOSP obtained by the Elovich model fitting are marginally higher than those of the OSP, and the *a* values of the dynamic adsorption are much larger than those of the static adsorption (Table 1), confirming that the MOSP had a relatively faster initial adsorption rate than the OSP, and the dynamic method was able to promote the adsorption process.

In static adsorption, the membrane PM and the adsorbent (i.e. the OSP and the MOSP) could be considered as a whole for the adsorption reaction because they are bound together. The overall adsorption process involved not only rate-limited chemisorption processes, such as interactions between the adsorbent and the adsorbent, electron sharing, or substitution, but also diffusion of the adsorbent through the permeable membrane and into the interior of the adsorbent [13]. The concentration of heavy metal ions entering the membrane at the beginning of the adsorption process increased rapidly with the rapid water uptake by the membrane, which might be related to the hydroxyl group with hydrophilicity in the PM. However, the shell powder

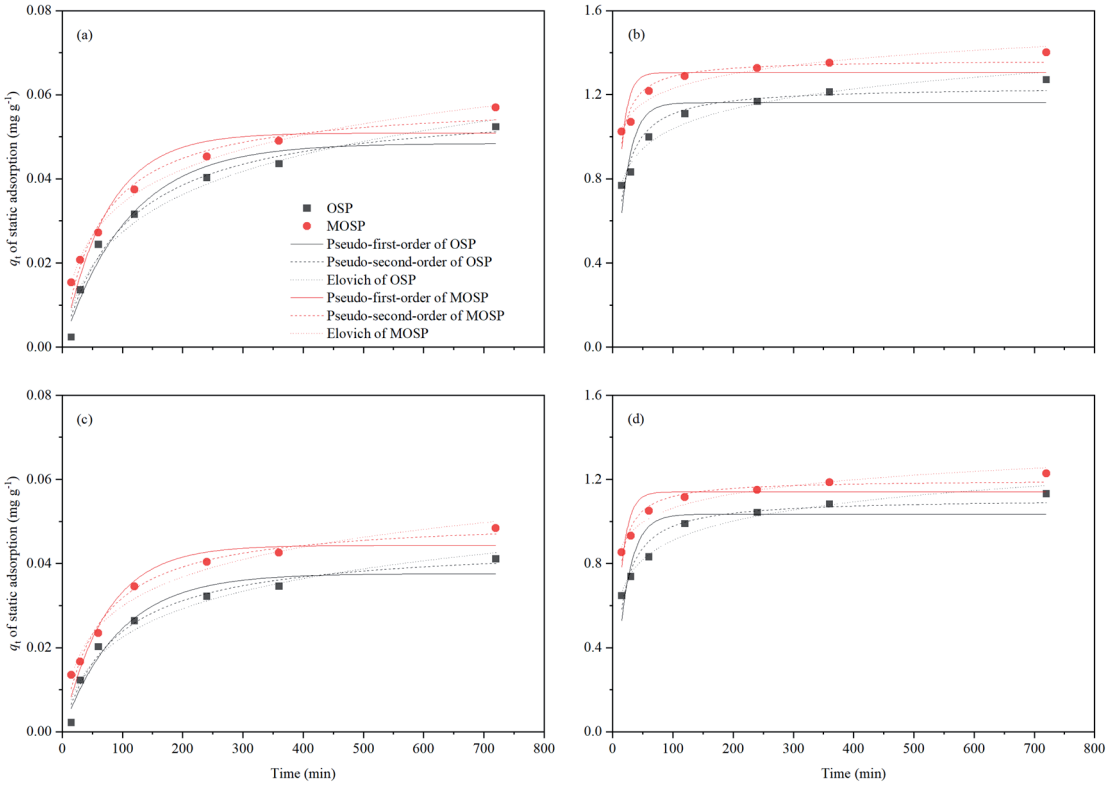

Fig. 5. Adsorption kinetics of Cu^{2+} (a, b) and Zn^{2+} (c, d) by the OSP (black square) and the MOSP (red dot) as well as the fitting curves of pseudo-first-order model (black and red solid line), pseudo-second-order model (black and red dashed line), and Elovich model (black and red dotted line). (a) and (c) represent static adsorption, (b) and (d) represent dynamic adsorption.

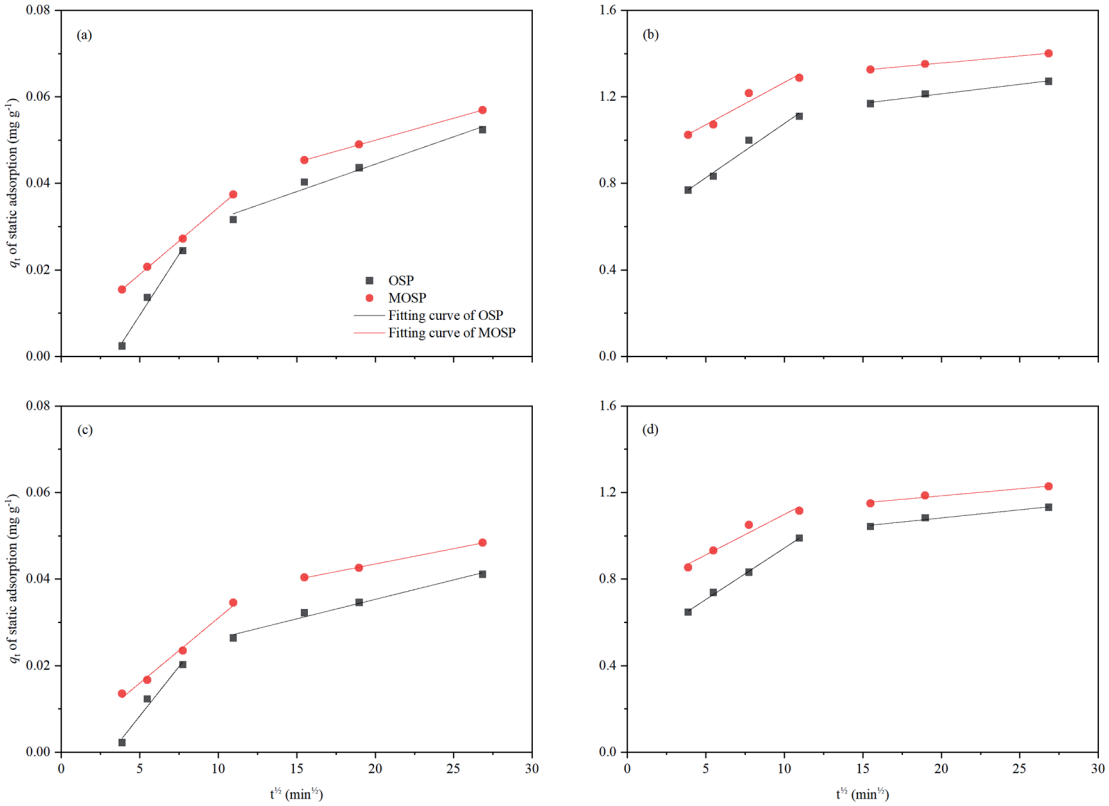

Fig. 6. Adsorption kinetics of Cu^{2+} (a, b) and Zn^{2+} (c, d) by the OSP (black square) and the MOSP (red dot) as well as the fitting curves of intraparticle diffusion model (black and red solid line). (a) and (c) represent static adsorption, (b) and (d) represent dynamic adsorption.

is liable to agglomerate and precipitate, which might hinder the diffusion of heavy metal ions to the surface of the adsorbent and the subsequent ion exchange [13, 14]. As a result, the adsorption capacity for Cu^{2+} and Zn^{2+} is relatively low when using the OSP. The dispersibility and hydrophilicity of the MOSP obtained by surface modification of the OSP were greatly increased, which improved the chance of an encounter between Ca^{2+} and the target ions, and ultimately increased the adsorption of Cu^{2+} and Zn^{2+} in the composites. In most adsorption processes, the adsorption reaction on the active site is relatively fast, and external/internal diffusion becomes the rate-controlling factor [30]. The pseudo models are generally used to discuss adsorption steps on the active site, while the intraparticle model is used for considering internal diffusion [35]. The kinetic models clearly illustrate that the adsorption processes of each heavy metal ion by different adsorbents have distinct stages, especially the intraparticle model. In the static adsorption, the rapid adsorption phase was relatively short. The shell powder agglomerates formed contained a large number of particles that did not undergo an adsorption reaction. However, the process of pollutant ions entering the interior structure of the agglomerates by diffusion was blocked, thus the external particle mass transfer began to slow down to gradually reach adsorption equilibrium.

When dynamic adsorption was performed, the adsorbent material circulated inside the membrane tube, and the heavy metal ions likewise passed through the PM membrane and came into contact with the adsorbent. As the adsorption materials underwent cyclic flow inside the membrane tube, the aggregation extent of the OSP decreased under mutual collision, and the chance of heavy metal ions meeting with the adsorbents was greatly increased. Therefore, the OSP could better perform the adsorption effect. A similar situation occurred with the MOSP. It can be explained that the dynamic running method facilitated the process of external substance mass transfer of pollutants to the adsorbent surface. The external mass transfer step plays an important role in the adsorption of pollutants on microplastics, especially for the MOSP particles with hydrate cover. Consideration from other perspectives, according to Bernoulli's principle, the flow of adsorbent inside the membrane tube led to a pressure drop, which might promote the mass transfer process of water and heavy metal ions through the PM. Compared with static adsorption, the OSP and the MOSP could provide better contact with target ions during dynamic adsorption and fully realize the adsorption effect. In other words, the OSP and the MOSP used in this study were far from saturated with adsorption, which may be the reason why the Elovich model is better applied.

Conclusions

In this study, a dynamic utilization method based on the modified adsorption material from waste shells was developed, which provides a feasible way for the application of oyster shell wastes for the remediation of heavy metal pollution in rural livestock and poultry wastewater. Fourier transform infrared spectroscopy (FT-IR), X-ray diffraction (XRD), and Scanning Electron Microscope (SEM) analyses showed that the modified adsorbent was successfully prepared. The results showed that the removal efficiency of heavy metal ions by the modified adsorbent material in the dynamic mode of operation was more than twenty times higher than that of the unmodified shell material in the static mode. This may be because surface modification improved the surface lubricity of the adsorbent material and, together with the dynamic adsorption method, avoided the occurrence of agglomeration of the adsorption material and enhanced the external mass transfer process. It should be noted that dynamic and static treatment methods can be used in conjunction with each other, e.g. dynamic treatment is a good choice when rapid treatment is required, but static adsorption can be used in the substrate for long-term treatment. In this study, the adsorbent material was collected directly to test the adsorption capacity, instead of calculating the amount of adsorption by the traditional way of collecting the supernatant. The reason for this approach is that the membranes and modified materials used have certain water absorption and the dynamic operation method also causes water and heavy metal ions to pass through the percolation membrane at different rates, and the results obtained by taking the supernatant directly are less accurate. Therefore, adsorption kinetics were not calculated in this study, which is an important issue to be addressed in future studies. Overall, the use of adsorbent materials made from oyster shell waste and dynamically operated adsorption as a cheap and easy-to-use treatment method shows the possibility of solving heavy metal pollution in livestock wastewater.

Acknowledgments

This work was financially supported by the Project of Talent Introduction and Education Program of Youth Innovation Teams in Universities of Shandong Province (2021-05), the Key Research and Development Project of Ningxia Hui Autonomous Region (2021BEG03013), and Innovation and Entrepreneurship Training Programme for College Students in Shandong Province (20210204153).

Conflict of Interest

The authors declare no conflict of interest.

References

1. ZHONG S., LI J., ZHANG D. Measurement of green total factor productivity on Chinese pig breeding: from the

perspective of regional differences. Environmental Science and Pollution Research. **29**, 27479, **2022**.
2. ZHOU K., WANG H., WU J., LI J. Effect of digital economy on large-scale pig farming: An empirical study from China. Cogent Food & Agriculture. **9** (1), 2238985, **2023**.
3. FAYAZ T., RENUKA N., RATHA S.K. Antibiotic occurrence, environmental risks, and their removal from aquatic environments using microalgae: Advances and future perspectives. Chemosphere. **349**, 140822, **2024**.
4. LI H., CHENG Y., LIU Y., LI S., HAN X., MA Y. Trace element accumulation from swine feeds to feces in Chinese swine farms: Implication for element limits. Integrated Environmental Assessment and Management. **18** (4), 978, **2022**.
5. PENG S., ZHANG H., SONG D., CHEN H., LIN X., WANG Y., JI L. Distribution of antibiotic, heavy metals and antibiotic resistance genes in livestock and poultry feces from different scale of farms in Ningxia, China. Journal of Hazardous Materials. **440**, 129719, **2022**.
6. ZHOU Z., WANG Y., SUN S., WANG Y., XU L. Preparation of PVA/waste oyster shell powder composite as an efficient adsorbent of heavy metals from wastewater. Heliyon. **8** (12), e11938, **2022**.
7. XIA C., ZHANG X., XIA L. Heavy metal ion adsorption by permeable oyster shell bricks. Construction and Building Materials. **275**, 122128, **2021**.
8. RAJAKARUNA R.M.A.S.D., SEWWANDI B.G.N., NAJIM M.M.M., BAIG M.B., ALOTAIBI B.A., TRAORE A. Sustainable Approaches for Wastewater Treatment: An Analysis of Sludge-Based Materials for Heavy Metal Removal from Wastewater by Adsorption. Sustainability. **15** (20), 14937, **2023**.
9. ZHANG Y., ZHANG L., GAO R., ZHONG L., XUE J. $CaCO_3$-coated PVA/BC-based composite for the simultaneous adsorption of Cu(II), Cd(II), Pb(II) in aqueous solution. Carbohydrate Polymers. **267**, 118227, **2021**.
10. PLAZINSKI W., RUDZINSKI W., PLAZINSKA A. Theoretical models of sorption kinetics including a surface reaction mechanism: A review. Advances in Colloid and Interface Science. **152** (1-2), 2, **2009**.
11. ESLAMI A., CHEGINI Z.G., KHASHIJ M., MEHRALIAN M., HASHEMI M. Removal of acetaminophen (ACT) from aqueous solution by using nanosilica adsorbent: experimental study, kinetic and isotherm modeling. Pigment & Resin Technology. **49** (1), 55, **2020**.
12. ESLAMI A., MEHRALIAN M., CHEGINI Z.G., KHASHIJ M. Application of nanosilica-based adsorbent for the removal of rhodamine B and methylene blue from aqueous solutions. Desalination and Water Treatment. **108**, 345, **2018**.
13. XU X., LIU X., OH M., PARK J. Oyster shell as a low-cost adsorbentfor removing heavy metal ions from wastewater. Polish Journal of Environmental Studies. **28** (4), 2949, **2019**.
14. PU L., XIE Y., QIU W., LI L. Thermoplastic foaming mechanism and Pb^{2+} adsorption of poly(vinyl alcohol)/shell powder porous composite. Polymer Composites. **40**, 4658, **2019**.
15. KIM W., SINGH R. Modified Oyster Waste Shells as a Value-Added Sorbent for Lead Removal from Water. Bulletin of Environmental Contamination and Toxicology. **108**, 518, **2022**.
16. YUE G.H., TAY Y.X., WONG J., SHEN Y., XIA J. Aquaculture species diversification in China. Aquaculture and Fisheries. **9** (2), 206, **2024**.
17. LIN C.-Y., DAI G.-L., LIU Y., ZHANG M.-Q., LIU Y., JIANG W., FU X.-M., CHEN H.-X. Ecological value of mariculture shellfish resources in China: Assessment and management. Marine Policy. **148**, 105406, **2023**.
18. IWASE K., HARUNARI Y., TERAMOTO M., MORI K. Crystal structure, microstructure, and mechanical properties of heat-treated oyster shells. Journal of the Mechanical Behavior of Biomedical Materials. **147**, 106107, **2023**.
19. KANG S.B., WANG Z., WON S.W. Polyethylenimine-crosslinked calcium silicate hydrate derived from oyster shell waste for removal of Reactive Yellow 2. Korean Journal of Chemical Engineering. **40**, 136, **2023**.
20. ALZIYADI M.O., GAMAL H., ALKABSH A., SHALABY M.S. Ex-situ synthesis, comprehensive characterization, and comprehensive properties of PVA film composites coated Spinel MgMn1.8Co0.2O4 nanoparticle. Applied Physics A. **130**, 320, **2024**.
21. ALHARTHI S.S., BADAWI A. Modification of the Structure and Linear/Nonlinear Optical Characteristics of PVA/Chitosan Blend through CuO Doping for Eco-Friendly Applications. Polymers. **15**, 2391, **2023**.
22. SONG Y., ZHANG S., KANG J., CHEN J., CAO Y. Water absorption dependence of the formation of poly(vinyl alcohol)-iodine complexes for poly(vinyl alcohol) films. RSC Advances. **11**, 28785, **2021**.
23. ZHU Y., LI Y., DING H., LU A., LI Y., WANG C. Multifactor-controlled mid-infrared spectral and emission characteristic of carbonate minerals (MCO_3, M=Mg, Ca, Mn, Fe). Physics and Chemistry of Minerals. **48**, 15, **2021**.
24. HAJJI S., TURKI T., BOUBAKRI A., AMOR M.B., MZOUGHI N. Study of cadmium adsorption onto calcite using full factorial experiment design. Desalination and Water Treatment. **83**, 222, **2017**.
25. WANG L.-Y., WANG M.-J. Removal of Heavy Metal Ions by Poly(vinyl alcohol) and Carboxymethyl Cellulose Composite Hydrogels Prepared by a Freeze−Thaw Method. ACS Sustainable Chemistry & Engineering. **4** (5), 2830, **2016**.
26. STREU K., HUNSBERGER S., PATEL J., WAN X., CLYDE A. DALY J. Development of a universal method for vibrational analysis of the terminal alkyne C≡C stretch. The Journal of Chemical Physics. **160**, 074106, **2024**.
27. MALLAKPOUR S., KHADEM E. Facile and cost-effective preparation of PVA/modified calcium carbonate nanocomposites via ultrasonic irradiation: Application in adsorption of heavy metal and oxygen permeation property. Ultrasonics Sonochemistry. **39**, 430, **2017**.
28. ELLERBROCK R., STEIN M., SCHALLER J. Comparing amorphous silica, short-range-ordered silicates and silicic acid species by FTIR. Scientific Reports. **12**, 11708, **2022**.
29. KHASHIJ M., SALMANI M.H., DALVAND A., FALLAHZADEH H., HAGHIROSADAT F., MOKHTARI M. ZnO-based nanocomposites for removal of lead (Pb^{2+}) from water/wastewater: a review. Pigment & Resin Technology. **52** (4), 456, **2023**.
30. WANG J., GUO X. Adsorption kinetic models: Physical meanings, applications, and solving methods. Journal of Hazardous Materials. **390**, 122156, **2020**.
31. VAREDA J.P. On validity, physical meaning, mechanism insights and regression of adsorption kinetic models. Journal of Molecular Liquids. **376**, 121416, **2023**.

32. KHASHIJ M., MOHAMMADI P., BABEI M., MEHRALIAN M., AGHAMOHAMMADI N. Process optimization and modeling of lead removal using maleate/PAN nanocomposite nanofibers: characterization, kinetics and isotherm studies. Desalination and Water Treatment. **210**, 330, **2021**.
33. KHASHIJ M., MOKHTARI M., DALVAND A., HAGHIRALSADAT F., FALLAHZADEH H., SALMANI M.H. Recycled PET/metal oxides nanocomposite membrane for treatment of real industrial effluents: Membrane fabrication, stability, antifouling behavior, and process modeling and optimization. Journal of Molecular Liquids. **364**, 119966, **2022**.
34. LAGOA R., RODRIGUES J.R. Kinetic analysis of metal uptake by dry and gel alginate particles. Biochemical Engineering Journal. **46** (3), 320, **2009**.
35. GUO X., WANG J. The phenomenological mass transfer kinetics model for Sr^{2+} sorption onto spheroids primary microplastics. Environmental Pollution. **250**, 737, **2019**.